




Article

Modeling Differential Pressure of Diesel Particulate Filters in Marine Engines

Jaehwan Jang ^{1,2,†}, Byungchae Min ^{1,†}, Seongyool Ahn ^{3,*}, Hyunjun Kim ^{4}, Sangkyung Na ¹, Jeongho Kang ^{4}, Heehwan Roh ² and Gyungmin Choi ^{1,*}

- ¹ School of Mechanical Engineering, Pusan National University, 2, Busandaehak-ro 63beon-gil, Geumjeong-gu, Busan 46241, Korea; jangjh@stxengine.co.kr (J.J.); byungchae.min@lge.com (B.M.); naskng@pusan.ac.kr (S.N.)
- ² STX Engine Co., Ltd., 36, Gongdan-ro 474beon-gil, Seongsan-gu, Changwon 51574, Gyengsangnam-do, Korea; myamo@stxengine.co.kr
- ³ Plant Engineering Center, Institute for Advanced Engineering, 175-28, Goanro 51, Yoingin 17180, Gyeonggi-do, Korea
- ⁴ Korea Automotive Technology Institute, 303, Pungse-ro, Pungse-myeon, Dongnam-gu, Cheonan-si 31214, Chungcheongnam-do, Korea; hjkim@katech.re.kr (H.K.); jhkang@katech.re.kr (J.K.)
- * Correspondence: syahn@iae.re.kr (S.A.); choigm@pusan.ac.kr (G.C.); Tel.: +82-31-330-7822 (S.A.); +82-51-510-2476 (G.C.)
- † These authors contributed equally to this work.

Abstract: The captured particulate matter (PM) in diesel particulate filters (DPF) must be periodically burned to maintain the performance and durability of the engine. The amount of PM in the filter must be monitored to determine a suitable regeneration period. In this study, the modeling parameters of the DPF were optimized using experimental data to determine a suitable regeneration period for the DPF for marine diesel engines. The differential pressure over the exhaust gas mass flow rate and temperature were measured using a fresh DPF. The modeling parameters of Darcy's law were optimized using the experimental data. Finally, the model parameters were validated using differential pressure data obtained from a DPF containing PM. The proposed model, which is a function of the gas flow rate, temperature, and amount of collected PM, was developed to simulate the differential pressure of DPFs and shows potential for application in the development of regeneration logic for marine DPFs.

Keywords: marine diesel engine; diesel particulate filter; after treatment; particulate matter; regeneration



Citation: Jang, J.; Min, B.; Ahn, S.; Kim, H.; Na, S.; Kang, J.; Roh, H.; Choi, G. Modeling Differential Pressure of Diesel Particulate Filters in Marine Engines. *Energies* **2022**, *15*, 3803. <https://doi.org/10.3390/en15103803>

Academic Editor: Constantine D. Rakopoulos

Received: 29 March 2022

Accepted: 18 May 2022

Published: 21 May 2022

Publisher's Note: MDPI stays neutral with regard to jurisdictional claims in published maps and institutional affiliations.



Copyright: © 2022 by the authors. Licensee MDPI, Basel, Switzerland. This article is an open access article distributed under the terms and conditions of the Creative Commons Attribution (CC BY) license (<https://creativecommons.org/licenses/by/4.0/>).

1. Introduction

As particulate matter (PM) regulations are strengthened worldwide, the necessity to reduce PM emissions from ships is increasing. Because diesel particulate filters (DPFs) use a physical filter to collect PM and reduce exhaust gas, the DPF backpressure increases with time, which can cause a decrease in engine output and an increase in fuel consumption. To eliminate PM from the DPF, the collected PM must be burned at regular intervals. In this burn-out process, the engine performance degradation can be minimized and the DPF lifetime can be maximized by selecting an appropriate regeneration time. Generally, the DPF usage time or engine idling pressure are the criteria used for determining the regeneration time because directly measuring the amount of PM in the DPF is difficult. To determine the optimal DPF regeneration time, technology that can accurately predict the amount of PM captured in the DPF is required [1,2].

Since Bissett proposed the nonlinear partial differential equation of the DPF model, various attempts have been made to predict the DPF differential pressure [3]. Jung et al. [4] developed a DPF filtration model based on experimental data of pressure variation and model parameter sensitivity. They found that the filtration trend and soot particle size were affected by the percolation constant and filtration quality, respectively. Mizutani

et al. [5] proposed a soot-regeneration model. This model is applicable to fuel additives and catalyst types. They investigated the engine performance and developed a safety soot regeneration model. Lee et al. [6] predicted the transient thermal response of the DPF. They considered the size and density of the DPF and the thermal response to soot loading. They found that increasing the cell density can decrease the maximum temperature owing to the increase in heat conduction and heat capacity. Muhammad et al. [7] investigated the regeneration characteristics of DPF. They used a computational method to evaluate the effect of exhaust flow on the DPF and analyzed the performance of the filter under transient exhaust conditions. Kazutake et al. [8] developed a newly designed DPF filter. They improved the ash capacity, and DPF lifetime by optimizing the inlet and outlet cell volumes. Additionally, they found that the octagon inlet form influenced soot filtration.

In previous studies, parameters such as the flow field and PM layer height have been utilized to predict the optimal regeneration time [9–13]. However, as technology has developed, the structure of the DPF has become more complex, and the scope of its application is expanding. To reflect this trend, an advanced DPF analysis model for the existing model is needed [14–19]. In this study, the optimal DPF regeneration time was suggested using Darcy's law's parameter, considering PM filtration and differential pressure behavior, based on the experimental data.

2. Experiment

2.1. Experimental Apparatus

2.1.1. Specification of Marine Engine

Figure 1 shows a photograph of the engine employed for the DPF test in this study. The engine is a 300 hp class diesel engine (D6DA) designed for a 300 ps class ship. The engine is a 6.6 L DI engine that produces a maximum output of 306 hp at 2500 rpm and satisfies Euro 3 regulations.

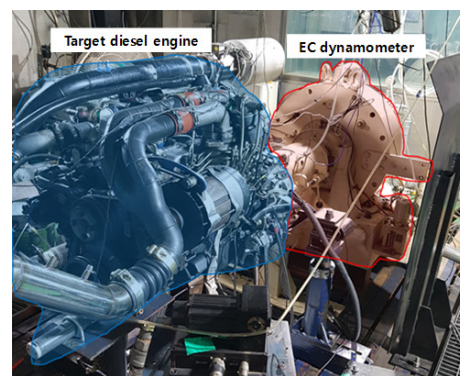


Figure 1. 300 hp diesel engine.

2.1.2. Diesel Particulate Filter (DPF)

Figure 2 shows the target system which is composed of a diesel oxidation catalyst (DOC) that increases the temperature for oxidation of unburned gas, and regeneration of the DPF and is designed to be used in engines with a maximum output of 300 hp. The DPF was supported by a cordierite-type catalyst with a cell density of 100 CPSI. Detailed specifications are listed in Table 1.

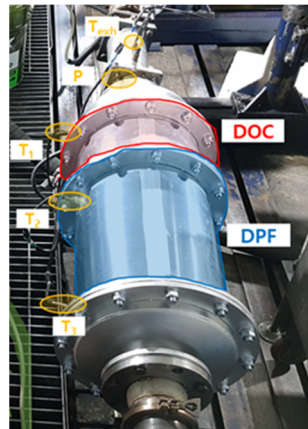


Figure 2. Target system: DOC and DPF.

Table 1. Specification of diesel particulate filter.

	Variable	Value	Unit
DPF	Filter type	Cordierite	
	Cell density	100	CPSI
	Substrate wall thickness	17.7	mil
	Monolith diameter	300	mm
	Monolith length	300	mm
	Plug length	20	mm
DOC	Filter type	Cordierite	
	Cell density	100	CPSI
	Monolith diameter	300	mm
	Monolith length	150	mm

2.2. Differential Pressure Test

2.2.1. Experimental Conditions

The zero-PM condition (0 g/L) was achieved by regenerating the DPF with sufficient time. To analyze the effect of the parameters and differential pressure considering temperature and flow rate, five different engine exhaust gas flow rates (250, 350, 450, 500, and 550 kg/h) and three temperatures (200, 300, and 400 °C) at the DPF inlet were considered. The engine operating conditions were adjusted to set the test conditions. The pressure was measured when the flow rate and temperature converged to the steady state under each condition.

2.2.2. Zero PM Condition

Figure 3 shows the results of the differential pressure of the zero-PM condition according to the temperature and flow rate change. The values of the differential pressure are distributed in the range of 7–33 mbar, as shown in the Figure 3 and Table 2. The differential pressure has a positive correlation with both the exhaust gas flow rate and exhaust gas temperature, and the increase in the flow rate when the temperature decreases has a great effect on the differential pressure. Under the same flow rate condition, the pressure change increases as the temperature increases because the DPF carrier cordierite expands as the temperature increases and the filter porosity decreases. High-speed and low-load operation of the engine is required to obtain a filter temperature of 200 °C and an exhaust gas flow rate of 550 kg/h. However, differential pressure data cannot be obtained under these conditions because the target engine has a minimum temperature of over 200 °C at an exhaust flow rate of 550 kg/h.

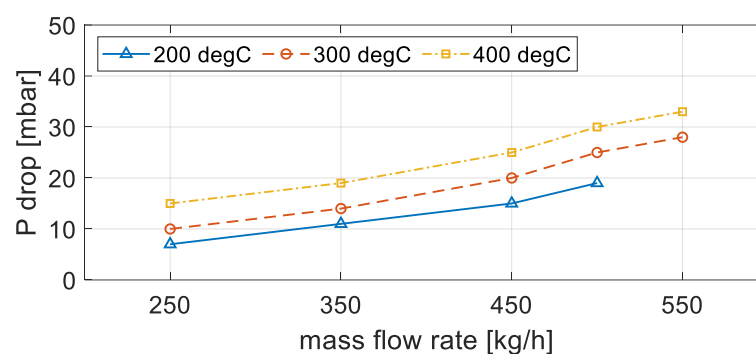


Figure 3. Differential pressure history at DPF with zero PM according to exhaust mass flow rate and exhaust temperature.

Table 2. Differential pressure values at DPF with zero PM condition.

DPF Inlet Temperature	Exhaust Mass Flow Rate	PM Mass	Differential Pressure
°C	kg/h	g/L	mbar
200	250	0	7
	350		11
	450		15
	500		19
	550		-
300	250		10
	350		14
	450		20
	500		25
	550		28
400	250		15
	350		19
	450		25
	500		30
	550		33

2.3. Effect of Captured PM

2.3.1. PM Capture

The effect of the captured PM on the differential pressure was investigated to validate the model, and the DPF differential pressure experiment was performed under the same conditions after the collection of the PM. For this purpose, PM was collected for 8 h at 1100 rpm and 260 Nm, which are the engine operating conditions for high PM emissions and no burning. The mass of DPF was measured five times before and after the PM collection, as shown in Table 3. The average mass before the collection was 85.880 kg and after the collection was 85.975 kg. In total, 95 g of PM was collected for 8 h, and it was calculated as the collection mass per DPF volume. Therefore, we collected approximately 4.27 g/L of PM.

Table 3. Mass of DPF: PM unloaded vs. loaded.

No.	Zero PM [kg]	4.27 g/L PM Loaded [kg]
1	85.893	85.979
2	85.876	85.961
3	85.872	85.967
4	85.878	85.985
5	85.883	85.985
Average	85.880	85.975

2.3.2. Differential Pressure Test with PM Capture

The differential pressure was measured under the same exhaust gas flow rates and DPF inlet temperatures mentioned in Section 2.2.1, as shown in Figure 4. In the case of DPF, in which PM of up to 4.27 g/L is collected, pressure varies between 15 and 45 mbar under the flow rate conditions shown in Table 4. When measuring differential pressures before and after the collection, the increase in the differential pressure was small at relatively high temperatures. At 200 °C, the differential pressure increased by 91.4% on average, whereas at 300 °C, the differential pressure increased by 59.4%. The parameters of the differential pressure model are optimized using the pressure data based on temperature and flow rate measured through this experiment.

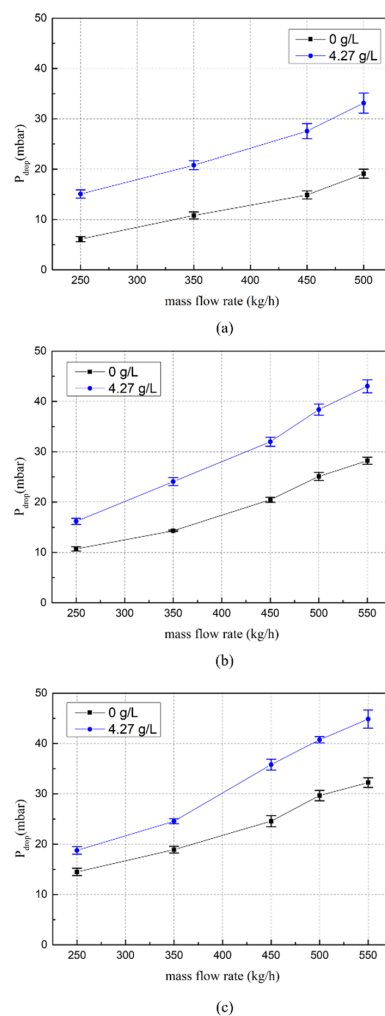


Figure 4. Differential pressure history at DPF with PM load of 4.27 g/L according to exhaust mass flow rate and exhaust temperature: (a) 200 °C; (b) 300 °C; (c) 400 °C.

Table 4. Result of differential pressure for PM load of 4.27 g/L.

DPF Inlet Temperature	Exhaust Mass Flow Rate	PM Load	Differential Pressure
°C	kg/h	g/L	mbar
200	250	4.27	15
	350		21
	450		28
	500		33
	550		-
300	250		16
	350		24
	450		32
	500		38
	550		43

3. Modeling of Differential Pressure Model

The differential pressure model has the advantage that it can estimate the pressure variations at the DPF under various exhaust conditions when the parameters set on the model are accurate, as shown in Tables 5 and 6. This model works based on Darcy's law by considering the PM layer and filter. The simulation was performed using the BOOST program (AVL List GmbH, Graz, Austria), which is a 1D simulator. The parameters of the differential pressure model for the DPF with the specifications in Table 1 were determined based on experimental data tested by considering the flow rate, temperature, and DPF loading condition of the exhaust gas [20].

Table 5. Parameters of differential pressure for clean DPF.

ζ_{inl}	4.78	
ζ_{out}	2.64	
k_w	200	6.23×10^{-11}
	300	6.27×10^{-13}
	400	4.48×10^{-13}

Table 6. Parameters of soot loading DPF differential pressure.

Soot Packing Density		100 kg/m ³
k_{sc}	200	2.3×10^{-14}
	300	3.6×10^{-14}
	400	5.9×10^{-14}

3.1. Differential Pressure Model

The modeled system of the BOOST program is illustrated in Figure 5. The system consists of a defining component as follows: the inlet and outlet boundary that defines the exhaust gas flow rate and temperature for the test, the DPF component that simulates the differential pressure according to the test condition, the diesel oxidation catalyst (DOC) component to which the Forchheimer differential pressure model is applied, and pipe components that connect the DOC and DPF parts.



Figure 5. The modeled system of BOOST program.

For the DPF differential pressure modeling based on the exhaust gas temperature, flow, and soot loading conditions, the differential pressure was measured under clean conditions, i.e., soot loading of between 0 and 4.27 g/L. The exhaust gas temperature at each soot loading condition and the flow rate were the same.

To create a DPF model that satisfies the differential pressure characteristics measured under the above conditions, both modeling and measurement comprise two steps. In the first step, a clean DPF differential pressure model is created for a soot loading of 0 g/L. In the second step, soot loading of 4.27 g/L was added to the DPF model completed in the first step, and the differential pressure characteristics caused by soot were modeled.

3.2. Clean DPF Modeling

The differential pressure of the DPF under clean conditions is shown in Figure 6. No. 1 and No. 7 in Figure 6 denote the exhaust gas flowing into the DPF inlet and exiting the outlet, respectively, resulting in a loss of inertia due to contraction/expansion at the DPF plug and inlet/outlet channels, as indicated by the numbers. It can be divided into pressure loss owing to frictional resistance, and that occurs while passing through the filter, as in No. 4.

$$\Delta p_{inl} = \zeta_{inl} \frac{\rho_{inl} v_{inl}^2}{2} \quad (1)$$

$$\Delta p_{out} = \zeta_{out} \frac{\rho_{out} v_{out}^2}{2} \quad (2)$$

$$\Delta p_{plug,inl} = \varphi \mu \frac{32 v_{inl}}{d_1^2} l_{plug} \quad (3)$$

$$\Delta p_{plug,out} = \varphi \mu \frac{32 v_{out}}{d_2^2} (l_{plug} + l_{ash}) \quad (4)$$

$$\Delta p_{channel,inl} = \frac{1}{l_{eff}} \int_0^{l_{eff}} [p_{g,1}(z=0) - p_{g,1}(z)] dz \quad (5)$$

$$\Delta p_{channel,out} = \frac{1}{l_{eff}} \int_0^{l_{eff}} [p_{g,2}(z) - p_{g,2}(z=l_{eff})] dz \quad (6)$$

$$\frac{\partial p_g}{\partial z} = -A_D v_g \quad (7)$$

$$A_D = \varphi \frac{v_g}{2} \frac{\rho_g}{d_{hyd}} \zeta = \varphi \frac{1}{2} \frac{\dot{m}}{A_{cross} d_{hyd}} \zeta \quad (8)$$

$$\Delta p_w = v_{w,1} \mu \frac{\rho_{g,1}}{\rho_{g,2}} \frac{\delta_w}{k_w} \quad (9)$$

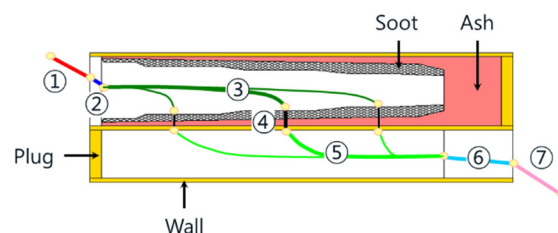


Figure 6. Schematic diagram of structure of pressure change.

The pressure loss caused by contraction/expansion at the DPF inlet and outlet is expressed in Equations (1) and (2). Here, ζ_{inl} and ζ_{out} are the friction loss coefficients, which are unknown variables for modeling the pressure loss of the DPF in this study. In Equations (1) and (2), the density and flow rate of the exhaust gas are determined using the temperature and flow rate, respectively, which are used as the test conditions in this study. As the density and flow rate increase, the pressure loss value increases. Similarly, the pressure loss value caused by contraction/expansion at the inlet and outlet of the DPF varies proportionally to the value of the friction loss coefficient, which is an unknown variable.

The pressure loss caused by the plug blocking the DPF inlet and outlet is expressed in Equations (3) and (4) [3]. Because of the absence of soot accumulation in the plug, Equations (3) and (4) can describe the pressure changes accurately. With respect to the pressure loss, the longer the plug length and the greater the exhaust gas flow rate and viscosity, the greater the pressure loss; whereas, the larger the channel diameter, the smaller the pressure loss. In the equations, φ denotes a shape factor of the channel for which a value of 1.05 is used as the shape of the DPF channel is square.

The pressure losses in the DPF inlet and outlet channels were calculated using Equations (5) and (6). Here, the pressure loss along the channel length is calculated using the steady-state Darcy model given in Equation (7); Equation (8) expresses the Darcy constant model. In this formula, DPF length is expressed as z . As the channel length, exhaust gas flow rate, and density increased, the pressure loss increased. However, as the channel diameter increased, the pressure loss decreased. Similar to the plug, the shape factor value of 1.05 was used for the channel as the shape of the DPF channel is square. As shown in Figure 2, when ash is accumulated in the inlet channel of the DPF, the pressure loss is calculated by subtracting the length of the ash from the length of the inlet and outlet channels. For the plug of the DPF outlet channel, the pressure loss is calculated using Equation (4), by adding the ash length [21].

The pressure loss caused by the exhaust gas passing through the DPF wall was calculated using the modified model of Darcy's law proposed by Konstandopoulos, as shown in Equation (9). For accurately predicting the pressure loss caused by the DPF wall, the model was developed using the measured data under the soot and ash loading conditions of 0 g/L. In Equation (9), K_w denotes the wall penetration area. The larger the K_w value, the larger the area through which the exhaust gas can pass; therefore, the calculated pressure loss is small. The K_w value depends on the filter material and production process. Because the DPF wall expands with the increase in temperature, independent K_w values must be used for each temperature. In this study, the differential pressure of the DPF was modeled using the K_w value, where various exhaust gas temperatures—200, 300, and 400 °C—were used as the parameter.

The analysis was performed under a soot loading of 0 g/L, as shown in Figure 3. Flow rate and temperature were set to be 3 °C/min. When the exhaust gas temperature in front of the DPF reaches 200 °C, the differential pressure is measured while increasing the flow rate from 250 to 550 kg/h. The x-axis in Figure 7 represents the test number, where 14 test conditions were used.

To create a DPF model that satisfies all 14 test conditions, shown in Figure 7, the inlet and outlet friction loss coefficients and K_w values for each temperature condition were determined as unknown variables, as listed in Table 2. To obtain the optimal unknown variable value, an AVL optimization software (Design Explorer) was used. Table 5 lists the unknown variables obtained using the optimization method.

The results in Table 5 show that the higher the exhaust gas temperature, the higher the DPF temperature and the smaller the wall penetration area because the filter expands owing to the characteristics of the DPF material. Therefore, under the same flow rate conditions, the differential pressure increased as the temperature increased. As the exhaust gas temperature increases, the differential pressure increases proportionally as the exhaust gas flow rate increases. Table 5 lists the unknown variables that account for these characteristics.

Among the unknown variables, the value of wall permeability at 200 °C is significantly larger compared to that at other temperatures. When wall permeability values between 300 and 400 °C were used, the value of differential pressure was overestimated compared to that obtained via measurement. The unknown variables were optimized within a range of 1–10.

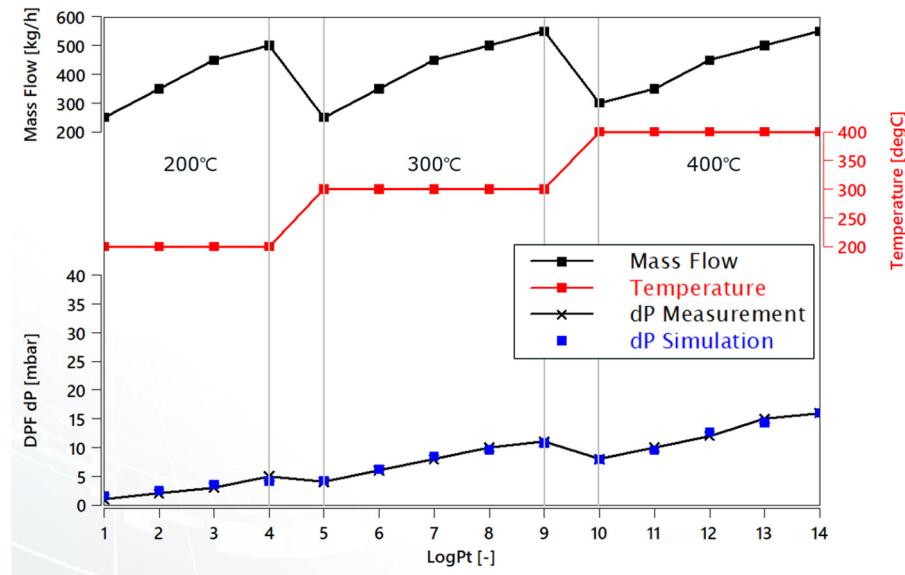


Figure 7. Differential pressure of clean DPF and boundary conditions.

The results presented in Figure 7 show that the simulation data are in good agreement with the measured data (dP of the DPF). The maximum error value obtained between the simulation and experimental data was less than 1×10^{-3} bar; therefore, the model is effective and can make accurate predictions.

Soot Loading

The more the soot is filtered in the DPF, the greater the amount of soot loading; because the soot acts as a filter, the filtration efficiency of the DPF improves but the differential pressure increases. To model the differential pressure characteristics according to soot loading, an engine dynamometer test was conducted in this study until the soot loading was ≥ 4 g/L. During the soot loading, the same exhaust gas temperature and flow conditions used for the clean DPF test were employed, and the differential pressure was measured.

The differential pressure owing to the soot cake was modeled using Equation (10). The modification was carried out using the test conditions and measured data presented in Figure 8. The unknown variables that were used for the modeling were the soot packing density (SPC) and K_{sc} . The SPC indicates the mass per unit volume and is used to calculate the volume according to the soot mass. The thickness of the soot layer was determined from these values. It is important to determine the optimal value because the effective diameter of the DPF channel depends on the thickness of the soot layer, and this affects the pressure loss [21].

$$\Delta p_{sc} = \frac{d_1}{2 \cdot K_{sc}} \cdot \ln \left(\frac{d_1 - 2 \cdot \delta_{ac}}{d_1 - 2 \cdot \delta_{sc} - 2 \cdot \delta_{ac}} \right) \quad (10)$$

In Equation (10), K_{sc} denotes the penetration area of the soot cake. As with K_w , the larger the K_{sc} value, the larger the area through which the exhaust gas can pass through the soot cake; thus, the calculated pressure loss is large. Further, the K_{sc} value varied depending on the engine.

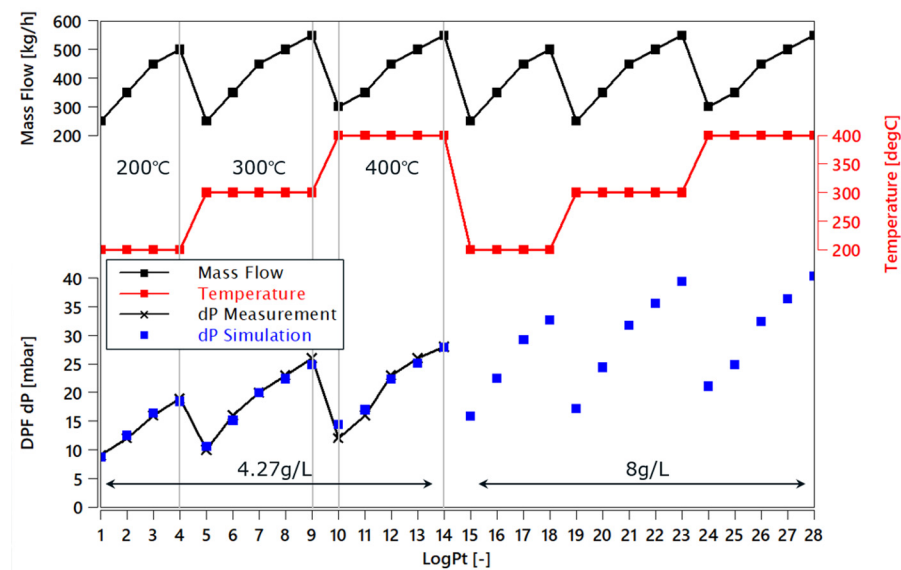


Figure 8. Differential pressure of 4.27 g/L Soot Loading DPF and Boundary Conditions.

In Equation (10), the DPF inlet channel diameter is the same as the ash cake thickness. In this study, as the differential pressure was measured in the absence of ash, it was not used in the differential pressure calculation. As the value of the soot cake thickness increases, the natural logarithmic value increases, and thus, the differential pressure increases. In addition, as the K_{sc} value also decreases, the calculated differential pressure is large.

Similar to Figure 7, the AVL optimization software Design Explorer was used to obtain the soot packing density and K_{sc} values that satisfy the differential pressure characteristics for conditions 1–14. Table 5 lists the unknown variables obtained using the optimization method.

The K_{sc} value obtained using the optimization technique increased as the temperature increased. Unlike filters, soot cake does not have expansion or contraction characteristics that depend on the temperature; therefore, soot undergoes passive regeneration at the time of the test, and it has a significant influence on the values of differential pressure. The K_{sc} had the largest value at 400 °C where passive regeneration occurred relatively often.

The result is similar to that of the dP of DPF in Figure 7; the measurement and analysis results were compared. The model showed an accuracy of within 1 mbar in all the conditions except for the 10th condition. As the test is completed in the 11–14th conditions, the decrease in soot is affected by the passive regeneration that occurred during the 11–14th tests. Therefore, in the 10th condition, the calculated analysis result was higher than the measurement result. In a future study, we plan to verify the results of this study by adding the passive regeneration model to the DPF model.

3.3. Differential Pressure at High Soot Loading

The effect of increasing soot loading on the differential pressure was calculated using the model with a soot loading of 8 g/L. The other conditions, such as the exhaust gas temperature and flow rate, were identical to those used in the other differential pressure tests. The obtained values are in the range of 15–18, as shown in Figure 8, which are compared to that of the case with a soot loading of 4.27 g/L. The results demonstrate that the effect of soot loading does not increase in proportion to soot loading because even though there is approximately 1.87 times the increase in soot loading, the differential pressure increases by approximately 1.6 times at 300 °C and 1.45 times at 400 °C. This is because the K_{sc} value becomes larger as the temperature increases, so the pressure decreases more at higher temperatures. When passive regeneration is considered, soot loading has a relatively large effect on the differential pressure.

4. Conclusions

In this study, the values of the major variables affecting the simulation of differential pressure, such as the permeabilities of the DPF filter and PM layer, were obtained through a correlation analysis between the experiment and the 1D model. Through this process, a numerical analysis technique that can predict differential pressure under various conditions was established using a high-quality 1D DPF model that was developed. The developed model can predict the differential pressure based on the exhaust gas flow rate, temperature, and DPF loading conditions. Consequently, the DPF specifications according to the PM collection conditions and various engine outputs can be determined at the initial-concept stage using a 1D model, which is advantageous in terms of cost and time.

Author Contributions: Conceptualization, J.J.; methodology, J.J. and H.R.; experiment, H.K. and J.K.; software, J.J., S.N. and H.R.; validation, J.J., S.N. and H.R.; formal analysis, J.J., B.M. and S.A.; investigation, J.J., S.N., H.R., B.M. and S.A.; resources, J.J. and B.M.; data curation, J.J., S.N., B.M. and S.A.; writing—original draft preparation, J.J.; writing—review and editing, S.A. and G.C.; supervision, S.A.; project administration, G.C.; funding acquisition, J.J. and H.R. All authors have read and agreed to the published version of the manuscript.

Funding: This study was supported by project ID PKN19AB of the Korea Industrial Complex Corporation (KICOX) and No. 22DPRB-C161884-02 of the Korea Agency for Infrastructure Technology Advancement (KAIA).

Institutional Review Board Statement: Not applicable.

Informed Consent Statement: Not applicable.

Data Availability Statement: Not applicable.

Conflicts of Interest: The authors declare no conflict of interest.

References

1. Jung, S.C.; Park, J.S.; Yoon, W.S. Rigorous Modeling of Single Channel DPF Filtration and Sensitivity Analysis of Important Model Parameters. *Trans. KSAE* **2006**, *14*, 127–136.
2. Yu, J.; Chun, J.R.; Hong, H.J. Prediction of Particulate Matter Being Accumulated in a Diesel Particulate Filter. *Trans. KSAE* **2009**, *17*, 29–34.
3. Bissett, E.J. Mathematical Model of the Thermal Regeneration of a Wall-flow Monolith Diesel Particulate Filter. *Chem. Eng. Sci.* **1984**, *39*, 1233–1244. [CrossRef]
4. Jung, S.C.; Park, J.S.; Yoon, W.S. Rigorous Modeling of Pressure Drops for Single Channel DPF Filtration. SAE Technical Papers. Gyunggido, Korea. 24–26 November 2005, pp. 408–415. Available online: <https://www.dbpia.co.kr/journal/articleDetail?nodeId=NODE00660013> (accessed on 10 May 2022).
5. Mizutani, T.; Watanabe, Y.; Yuuki, K.; Hashimoto, S.; Hamanaka, T.; Kawashima, J. Soot Regeneration Model for SiC-DPF System Design. In Proceedings of the SAE 2004 World Congress & Exhibition, Detroit, MI, USA, 8–11 March 2004. [CrossRef]
6. Lee, S.J.; Jeong, S.J.; Kim, W.S. Numerical Design of the Diesel Particulate Filter for Optimum Thermal Performances during Regeneration. *Appl. Energy* **2009**, *86*, 1124–1135. [CrossRef]
7. Khan, M.R.; Shamim, T. Regeneration Characteristics of Diesel Particulate Filters Under Transient Exhaust Conditions. In Proceedings of the International Combustion Engine Division Spring Technical Conference, Chicago, IL, USA, 27–30 April 2008; pp. 107–115.
8. Ogyu, K.; Ohno, K.; Hong, S.; Komori, T. Ash Storage Capacity Enhancement of Diesel Particulate Filter. *SAE Trans.* **2004**, *113*, 466–473.
9. Huynh, C.T.; Johnson, J.H.; Yang, S.L.; Bagley, S.T.; Warner, J.R. A One-dimensional Computational Model for Studying the Filtration and Regeneration Characteristics of a Catalyzed Wall-flow Diesel Particulate Filter. *SAE Trans.* **2003**, *112*, 620–646.
10. Tan, J.C.; Opris, C.N.; Baumgard, K.J.; Johnson, J.H. *A Study of the Regeneration Process in Diesel Particulate Traps Using a Copper Fuel Additive*; Society of Automotive Engineers, Inc.: Warrendale, PA, USA, 1996.
11. Koltsakis, G.; Haralampous, O.; Depcik, C.; Ragone, J.C. Catalyzed Diesel Particulate Filter Modeling. *Chem. Eng.* **2013**, *29*, 1–61. [CrossRef]
12. Punke, A.; Grubert, G.; Li, Y.; Dettling, J.; Neubauer, T. Catalyzed Soot Filters in Close Coupled Position for Passenger Vehicles. In Proceedings of the SAE 2006 World Congress & Exhibition, Detroit, MI, USA, 3–6 April 2006. [CrossRef]
13. Kuwahara, T.; Yoshida, K.; Kuroki, T.; Hanamoto, K.; Sato, K.; Okubo, M. High Reduction Efficiencies of Adsorbed NO_x in Pilot-Scale Aftertreatment Using Nonthermal Plasma in Marine Diesel-Engine Exhaust Gas. *Energies* **2019**, *12*, 3800. [CrossRef]

14. Zokoe, J.; Su, C.; McGinn, P.J. Soot Combustion Activity and Potassium Mobility in Diesel Particulate Filters Coated with a K-Ca-Si-O Glass Catalyst. *Ind. Eng.* **2019**, *58*, 11891–11901. [[CrossRef](#)]
15. Engelmann, D.; Zimmerli, Y.; Czerwinski, J.; Bonsack, P. Real Driving Emissions in Extended Driving Conditions. *Energies* **2021**, *14*, 7310. [[CrossRef](#)]
16. Du, Y.; Hu, G.; Xiang, S.; Zhang, K.; Liu, H.; Guo, F. Estimation of the Diesel Particulate Filter Soot Load Based on an Equivalent Circuit Model. *Energies* **2018**, *11*, 472. [[CrossRef](#)]
17. Ge, J.C.; Choi, N.J. Soot Particle Size Distribution Regulated and Unregulated Emissions of a Diesel Engine Fueled with Palm Oil Biodiesel Blends. *Energies* **2020**, *13*, 5736. [[CrossRef](#)]
18. Jarosiński, W.; Wiśniowski, P. Verifying the Efficiency of a Diesel Particulate Filter Using Particle Counters with Two Different Measurements in Periodic Technical Inspection of Vehicles. *Energies* **2021**, *14*, 5128. [[CrossRef](#)]
19. Verma, P.; Stevanovic, S.; Zare, A.; Dwivedi, G.; Chu Van, T.; Davidson, M.; Rainey, T.; Brown, R.J.; Ristovski, Z.D. An Overview of the Influence of Biodiesel, Alcohols and Various Oxygenated Additives on the Particulate Matter Emissions from Diesel Engines. *Energies* **2019**, *12*, 1987. [[CrossRef](#)]
20. Beller, G.; Arpad, I.; Kiss, J.T.; Kocsis, D. AVL BOOST: A Powerful Tool for Research and Education. *J. Phys. Conf. Ser.* **1935**, 012015. [[CrossRef](#)]
21. Wirojsakunchai, E.; Schroeder, E.; Kolodziej, C.; Foster, D.E.; Schmidt, N.; Root, T.; Kawai, T.; Suga, T.; Nevius, T.; Kusaka, T. Detailed Diesel Exhaust Particulate Characterization and Real-Time DPF Filtration Efficiency Measurements During PM Filling Process. In Proceedings of the SAE World Congress & Exhibition, Detroit, MI, USA, 16–19 April 2007. [[CrossRef](#)]